Quantum Information and Computation, Vol. 9, No. 3&4 (2009) 0203–0214

SCALABLE, EFFICIENT ION-PHOTON COUPLING WITH PHASE FRESNEL LENSES FOR LARGE-SCALE QUANTUM COMPUTING

E.W. STREED, B.G. NORTON, J.J. CHAPMAN, and D. KIELPINSKI
Centre for Quantum Dynamics, Griffith University
Nathan, QLD 4111, Australia

Received May 20, 2008
Revised November 12, 2008

Efficient ion-photon coupling is an important component for large-scale ion-trap quantum computing. We propose that arrays of phase Fresnel lenses (PFLs) are a favorable optical coupling technology to match with multi-zone ion traps. Both are scalable technologies based on conventional micro-fabrication techniques. The large numerical apertures (NAs) possible with PFLs can reduce the readout time for ion qubits. PFLs also provide good coherent ion-photon coupling by matching a large fraction of an ion's emission pattern to a single optical propagation mode (TEM_{00}). To this end we have optically characterized a large numerical aperture phase Fresnel lens (NA=0.64) designed for use at 369.5 nm, the principal fluorescence detection transition for Yb^+ ions. A diffraction-limited spot $w_0 = 350 \pm 15$ nm ($1/e^2$ waist) with mode quality $M^2 = 1.08 \pm 0.05$ was measured with this PFL. From this we estimate the minimum expected free space coherent ion-photon coupling to be 0.64%, which is twice the best previous experimental measurement using a conventional multi-element lens. We also evaluate two techniques for improving the entanglement fidelity between the ion state and photon polarization with large numerical aperture lenses.

Keywords: trapped ion quantum computing, phase Fresnel lens, coherent coupling, diffractive optics, large aperture optics
Communicated by: D Wineland & R Blatt

1 Introduction

Quantum information processing leverages properties of quantum physics to perform computational and communications tasks with better scaling properties [1, 2] or with greater security [3] than classical techniques. Interest in this area has been stimulated by Shor's algorithm [1] for efficient factoring of large numbers, since modern public key encryption schemes rely on the intractability of this problem with classical computational algorithms. The electronic and motional states of trapped ions are one of the leading systems for realizing quantum information processing. Trapped ions have long coherence times, strong yet controllable inter-qubit coupling, and are easy to prepare, manipulate, and read out using established optical and microwave techniques. Many small-scale quantum computation tasks have been demonstrated with trapped ions [4, 5, 6, 7, 8] and a roadmap exists for larger scale architectures [9, 10, 11]. A common thread in all the proposed large scale ion trap quantum computing architectures is the need for a scalable, efficient method for collecting ion fluorescence. Arrays of phase Fresnel lenses (PFLs) are well suited to meeting these requirements because of their large numerical apertures and scalable production via conventional micro-fabrication techniques. Fig. 1 illustrates the integration of a PFL array with a multi-zone ion trap to create a high-density

quantum processor.

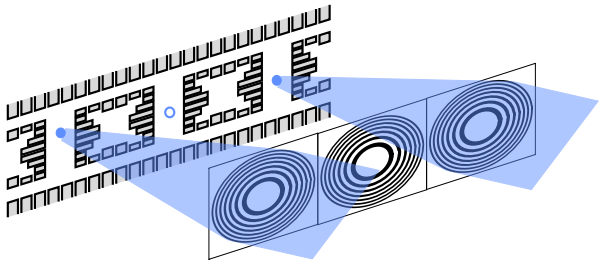

Fig. 1. Schematic of parallel optical operations on a multi-zone ion chip trap using an array of phase Frensel lenses.

PFLs are diffractive optical elements manufactured using conventional electron beam nanolithographic techniques. PFLs achieve diffraction-limited performance at high numerical apertures because on-axis geometrical aberrations are completely removed as part of the design process. Diffraction-limited performance with large numerical apertures (NA=0.9, 28% coverage of the total solid angle) has been demonstrated [12] in the near UV. At large NAs (> 0.5) the ion emission pattern ceases to resemble a point source and exhibits polarization dependent structure. PFLs offer design flexibility for mode matching between a specific emission pattern and a single optical spatial mode (TEM_{00}), maximizing the coherent coupling. While the diffraction efficiency of a high-NA multilevel PFL was previously thought to be limited to 20% at deflection angles near 45°, recent vector diffraction modeling of PFLs [13] shows efficiencies of 63% could be obtained in this regime with a modified groove structure. The modeling also indicates that coating PFLs with a 20 nm layer of indium tin oxide, sufficient to reduce the surface sheet resistance to 1kΩ/square [14], would reduce the diffraction efficiency by only 12%, mostly from absorption. In this paper we characterize the optical properties of an NA=0.64 phase Frensel lens. In future experiments this PFL will be inserted into a Yb^+ ion trap system for proof of concept demonstration. From these measurements we calculate the expected coherent coupling efficiency between the spontaneous emission from single ion and a fundamental gaussian mode (TEM_{00}), which is equivalent to the efficiency for coupling into a cavity or a single mode fiber. We also evaluate potential limitations specific to PFLs for several atom-photon entanglement schemes. In addition, we propose two solutions to entanglement fidelity limitations arising from the use of high-NA collection optics in an especially useful atom-photon entanglement scheme.

2 Experimental

The PFL (Fig. 2) was fabricated by electron-beam lithography on a fused silica substrate at the Fraunhofer-Institut für Nachrichtentechnik in Germany. The e-beam patterning defined series of rings of radius $r_p^2 = 2fp\lambda + p^2\lambda^2$, corresponding to contours with a π phase step, according to the scalar design equation for a binary PFL. Here $f = 3$ mm is the design focal length,p is the ring index number, and $\lambda = 369.5$ nm, the design wavelength, is the wavelength of the $S_{1/2}$-$P_{1/2}$ cycling transition in Yb^+. The rings were etched to a depth of 390 nm, shifting the optical path length in the etched zones by half a wavelength. The lens

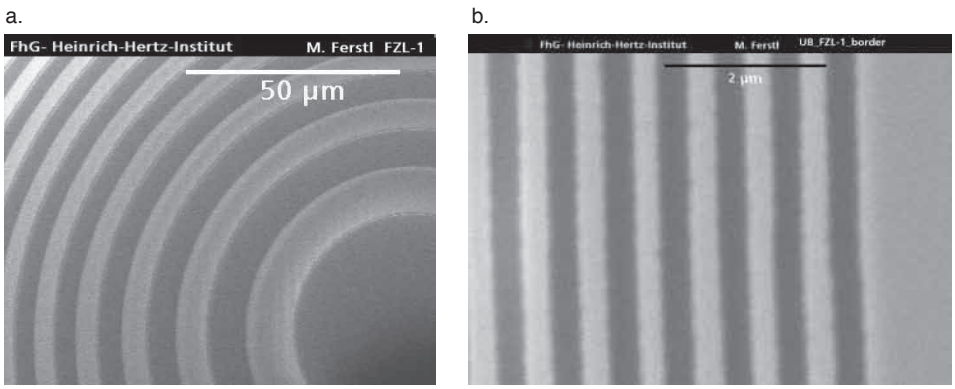

Fig. 2. Electron microscopy images of the patterned phase Fresnel lens surface. a. Center region showing the innermost rings. b. Edge region with structures of comparable size to the $\lambda = 369.5$ nm design wavelength. Images courtesy of M. Ferstl, Heinrich-Hertz-Institut of the Fraunhofer-Institut für Nachrichtentechnik.

clear aperture of 5 mm gives the lens a speed of F/0.6 and a NA=0.64, which corresponds to 12% of the total solid angle since $NA \equiv \sin\theta_{\max}$ in vacuum (index of refraction n=1) and so $NA = \frac{1}{\sqrt{1+4(F/\#)^2}}$. For small NA ($\theta_{\max} < 0.3$) the approximation $NA \approx \frac{1}{2F/\#}$ is often used, but is not valid in the high NA regime of interest. Aspheric lenses are often specified using the approximate NA formula even outside its range of validity, leading to grossly overstated catalog NA values.

Using a previously developed sub-micron beamprofiler [15], the focusing properties of this NA=0.64 binary PFL were measured using the knife edge technique. The focused beam is chopped by a razor blade oriented perpendicular to the optical axis and the optical power transmission as a function of position is fitted to determine the beam size. We define the beam waist w_0 as the $1/e^2$ intensity radius. Sub-micron accuracy in measuring the beam waist is realized with monitoring of the razor blade position by a Michelson interferometer. Fig. 3 shows a series of beam size measurements near the focus of the PFL given an input beam at the design wavelength and an input beam waist of 1.1 mm. The data was fitted to

$$w^2(z) = w_0^2 + M^4 \times \left(\frac{\lambda}{\pi w_0}\right)^2 z^2 \tag{1}$$

resulting in a minimum beam waist of $w_0 = 350 \pm 15$ nm and a beam propagation factor $M^2 = 1.08 \pm 0.05$, indicating almost ideal gaussian behavior. The fitted beam waist value w_0 was also verified against the actual experimental data to prevent inadvertent "false fitting" of an unobserved lower beam waist. The beam propagation factor M^2 represents the increase in beam divergence over that for an ideal gaussian beam of equal waist size and is defined through the equation [16]

The overall diffraction efficiency of the PFL into the focus was measured to be $\bar{\eta}_{\text{diff}} = 30 \pm 1\%$ of input power, comparable to the ideal efficiency of 37% (including Fresnel reflection losses) for a binary phase Fresnel lens. The total transmission was $92 \pm 1\%$, in agreement

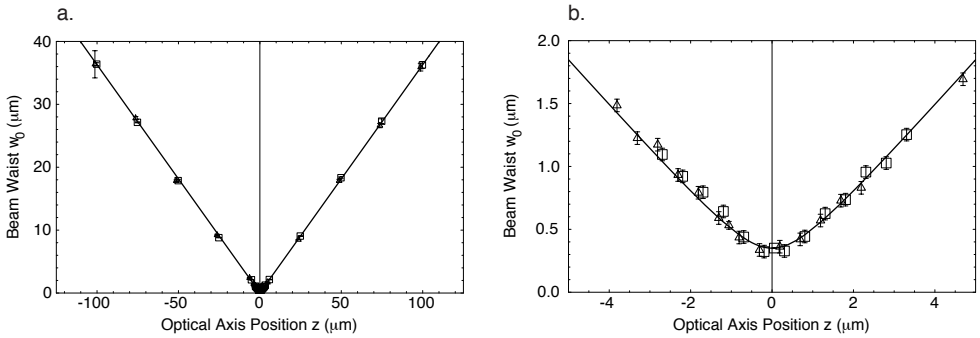

Fig. 3. Focusing performance of a large aperture (NA=0.64) binary phase Fresnel lens, 5 mm diameter clear aperture and 3 mm focal length with a 2.2 mm diameter input beam. a. Beam waist size as a function of position along the optical axis (z). b. Detail of focusing region from a. Fit curve is to Eq. 1 with $w_0 = 350 \pm 15$ nm and $M^2 = 1.08 \pm 0.05$. The half angle of the beam divergence is $\theta = 348 \pm 1$ mrad and the nominal Rayleigh range $z_R = \pi w_0^2/\lambda = 1040 \pm 90nm$. Data was taken with the knife edge moving in (triangles) and out (squares) of the beam. An imperfection in the translation stage resulted in a systematic shift of 1.11 ± 0.05 μm between the z location of the in and out curves. This artifact has been removed from the plotted data.

with the expected losses from Fresnel reflections (4% per surface) for a flat fused silica plate.

3 Analysis

3.1 Coupling efficiency

In an ion-trap quantum computer, light from an ion is either collected and detected or coupled into a subsequent optical device such as a single mode fiber, Fabry-Perot cavity, or interferometer. The probability that a photon is successfully collected by a lens

$$p_{coll} = f_{\text{orient, pol}}\,(\theta_{\max}) * \bar{\eta}_{\text{diff}} \tag{2}$$

depends on its average efficiency ($\bar{\eta}_{\text{diff}}$), numerical aperture (NA or $\theta_{\max}$), the transition polarization (σ or π), and the viewing orientation. The beam quality produced by the coupling optic is unimportant in photon counting applications so long as the collected light falls on the detector's active area. However, the probability that light from an ion is coherently coupled into a single optical mode

$$p_{coh} = f_{\text{orient, pol}}\left(\theta \frac{1}{M}\frac{\sqrt{2}}{2}\right) * \bar{\eta}_{\text{diff}} \tag{3}$$

does depend on the spatial quality of the beam (beam propagation factor M^2) which can be obtained for a particular beam divergence θ. The coherent ion-photon coupling can be estimated by approximating the measured beam as an ideal gaussian, normalizing the intensity with the top hat approximation, and applying this effective divergence angle $\theta_e = \theta/(M\sqrt{2})$ to a polarization and orientation dependent formula for the fraction of light emitted into a cone. The actual beam can be approximated as an ideal gaussian with its divergence angle reduced by $1/M$ from the measured divergence $\theta = 348 \pm 1$ mrad. The coherent coupling p_{coh}

of a spontaneously emitted photon into a single TEM_{00} optical mode is calculated according to Eq. 3, where $\bar{\eta}_{\mathrm{diff}}$ is the overall diffraction efficiency. The error introduced by applying the top hat approximation is less than 2% for divergences of less than 0.93 radians (NA<0.8 for a beam diameter equal to the clear aperture). This is in contrast to the collection efficiency (Eq. 2) which depends only on the maximum collection angle $\theta_{\max}$ (or NA) and the overall diffraction efficiency.

$$f_{p\sigma,e\pi}(\theta_m) = \tfrac{1}{2} - \tfrac{7}{16}\cos\theta_m - \tfrac{1}{16}\cos 2\theta_m \approx \frac{3}{8}\mathrm{NA}^2 + \frac{1}{64}\mathrm{NA}^6 \quad (4)$$

$$f_{e\sigma}(\theta_m) = \tfrac{1}{2} - \tfrac{17}{32}\cos\theta_m + \tfrac{1}{32}\cos 2\theta_m \approx \frac{3}{16}\mathrm{NA}^2 + \frac{3}{32}\mathrm{NA}^4 + \frac{5}{128}\mathrm{NA}^6 \quad (5)$$

$$f_{p\pi}(\theta_m) = (2+\cos\theta_m)\sin^4\tfrac{\theta_m}{2} \approx \frac{3}{16}\mathrm{NA}^4 + \frac{1}{16}\mathrm{NA}^6 \quad (6)$$

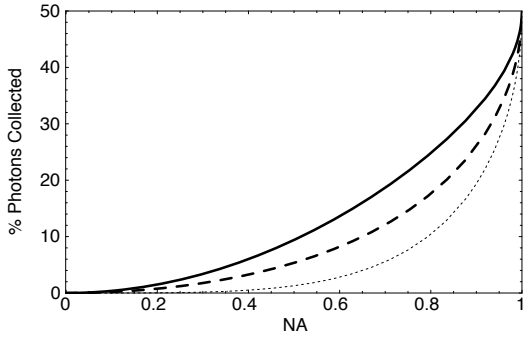

Fig. 4. Fraction of light captured as a function of lens NA. Solid black line (upper) is for Eq. 4, a π transition oriented along equator (optical axis perpendicular to magnetic field) and σ transitions oriented along the pole (optical axis parallel with magnetic field). Dashed line (middle) is Eq. 5, σ light from equatorial orientation. Dotted line (lower) is Eq. 6, π transition light from polar orientation.

We have calculated the emission collection fraction $f(\theta_m)$ as a function of acceptance angle for two different optical orientations (Fig. 4); the magnetic field parallel to the optical axis (a polar view in spherical coordinates) and the magnetic field perpendicular to the optical axis (equatorial view). For a polar view such as used in [18] the collection fraction is given by Eq. 4 for $\sigma^{\pm}$ transitions and Eq. 6 for π transitions. For an equatorial view, such as used in [8, 17], the collection fraction is given by Eq. 5 for $\sigma^{\pm}$ transitions and given by Eq. 4 for the π transition. Even though the emission pattern is different for polar/σ and equatorial/π, the fraction of light captured in an acceptance cone of angle θ_m is identical. The numerical aperture approximations are valid within 2% for NA<0.8.

For capturing photons in the most favorable conditions ($\sigma^{\pm}$ from a polar perspective, or π from an equatorial perspective) the coherent coupling of the characterized PFL is $p_{coh} \geq 0.64\%$, given diffraction-limited performance at the effective divergence angle $\theta_e = 246$ mrad and the measured 30% focusing efficiency. A higher-efficiency blazed PFL [13] would at least double this to $p_{coh} \geq 1.3\%$. The actual p_{coh} may be higher than this estimate as the optimum

tradeoff between lower M^2 and greater aperture will be determined *in situ*. From the measured diffraction efficiency and the lens NA the photon collection efficiency should be p_{coll} =4.6%. For comparison, in recent remote ion entanglement experiments [17, 18] the coherent coupling was p_{coh} ≈0.32%, as estimated from the lens numerical aperture and coupling efficiencies stated in the literature. The robust detection scheme used in these experiments requires interference of two fluorescence photons from the two ions at a beamsplitter and subsequent coincident detection. The photons only interfere if they are in the same spatial mode, making the coherent coupling efficiency p_{coh} rather than the collection efficiency p_{coll} the relevant measure of optical detection effictiveness. For perfect interference, the entanglement rate scales as p_{coh}^2, so the use of diffraction-limited high-NA optics such as PFLs promises great benefits.

3.2 Entanglement with $\sigma^{\pm}$ transitions

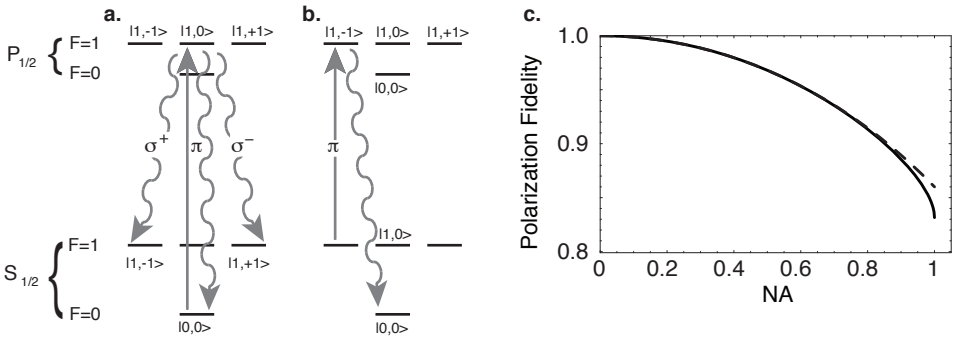

Fig. 5. a. π transition to excited state. Note that selection rules prevent a π photon emission at the same frequency as the $\sigma^{\pm}$ photons. b. Optical pumping back to F=0,m$_F$=0 state. For clarity only the primary pumping process for one part of the entangled state superposition is shown. c. Polarization fidelity of $\sigma^{\pm}$ photons in a polar view as a function of numerical aperture. Minimum fidelity is 0.832 at NA=1.0. Dashed line is the approximation $F(\mathrm{NA}) \approx 1 - \mathrm{NA}^2/8 - \mathrm{NA}^4/96 - 7\mathrm{NA}^6/1536$, valid to <1% for NA<0.95.

We now consider a specific ion-photon entanglement scheme based on $\sigma^{\pm}$ Raman transitions in $^{171}\mathrm{Yb}^+$. This configuration was recently used as part of a demonstration of Bell inequality violation between two remotely entangled ions [18]. Consider an ion initialized in the $\mathrm{S}_{1/2}$ $|0,0\rangle$ ($|F, m_F\rangle$) ground state. A laser drives the π polarized transition into the $\mathrm{P}_{1/2}$ $|1,0\rangle$ (Fig. 5a) excited state, with three possible decay channels. The ion can return to the $|0,0\rangle$ ground state via a Rayleigh scattered π polarized photon with 1/3 probability. Alternatively the ion can Raman scatter into the $|1,+1\rangle$ or $|1,-1\rangle$ states with a σ^+ or σ^- polarized photon, each with probability 1/3, which is frequency shifted from the excitation laser by 12.6 GHz (the ground state hyperfine splitting in $^{171}\mathrm{Yb}^+$). A collection optic oriented for viewing parallel to the magnetic field (polar orientation) will gather mostly $\sigma^{\pm}$ photons (Eq. 4) as the dipole radiation pattern of the π transition is suppressed in this direction (Eq. 6 and Fig 4). In this orientation the $\sigma^{\pm}$ photons appear to be circularly polarized and can be converted to linear polarization with a quarter-wave plate. Further suppression of the unwanted π photons at

large NA can be obtained with a Fabry-Perot etalon that selectively transmits the Raman shifted $\sigma^{\pm}$ photons. A factor of 1000 in suppression can be obtained with an etalon of finesse 50 and a free spectral range (FSR) of twice the Raman shift (25.3 GHz). After the entangling step two π pulses transfer the $|1,1\rangle$ and $|1,-1\rangle$ states to the magnetically insensitive clock states $|1,0\rangle$ and $|0,0\rangle$ for storage or detection, assuming the presence of a magnetic field to lift the Zeeman degeneracy.[a] To complete the cycle the ion can be reinitialized to the $|0,0\rangle$ state with an optical pumping step (Fig. 5b). This scheme generates an entangled ion-photon pair 2/3 of the time for a single scattering cycle and has excellent suppression of unwanted π photons.

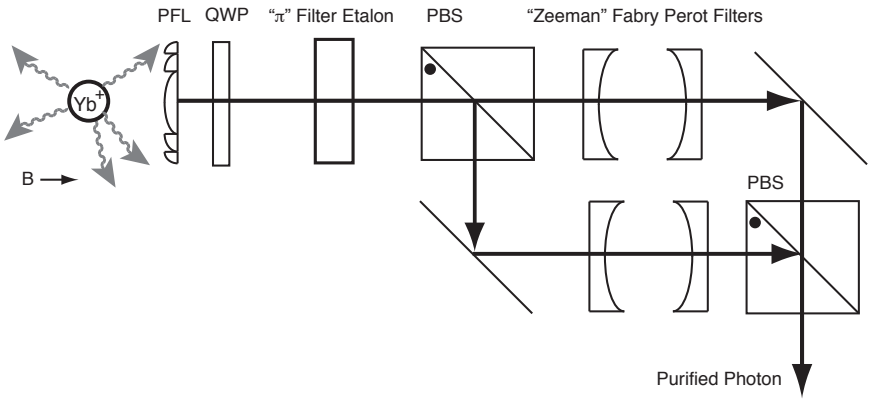

Fig. 6. Ion-photon entanglement with photon state filtering. Light from a Yb^+ ion in a magnetic field B is collimated by a PFL and σ photons are converted from circular to linear polarization by a quarter waveplate QWP. A 25.3 GHz free spectral range (FSR) "π" etalon is tuned to suppress unwanted π photons from the 12.6 GHz Raman shifted σ photons. A polarizing beamsplitter separates the two different linear polarizations for frequency dependent filtering based on the Zeeman splitting from the magnetic field. The two "Zeeman" Fabry-Perot filters are tuned to transmit only photons with the correct frequency for their polarization. A second polarizing beamsplitter recombines the two paths and completes the polarization interferometer.

Polarization contrast reduction (blurring) between σ^+ and σ^- photons at large angles is an additional source of error that becomes prominent with large numerical aperture optics. The polarization fidelity of a σ photon emitted at an angle θ from the optical axis drops as $\sqrt{1-\frac{1}{2}\sin^2\theta}$. As a function of NA the polarization fidelity of captured photons is plotted in Fig. 5 c. as determined by weighting the emission angle dependent fidelity by the emission probability distribution for a σ transition. Because of this blurring achieving ion-photon entanglement fidelity of greater than 99% is limited to collection optics with NA< 0.27, while a $>$90% fidelity requires NA < 0.85. Fortunately the photon state can be purified with the application of a magnetic field to resolve the Zeeman levels. Photons that are measured with the "wrong" polarization can be filtered out in the frequency basis by a pair of Fabry-Perot

[a] A straightforward implementation of this swap can be performed with a microwave sweep over the hyperfine transitions inducing three consecutive adiabatic Landau-Zener state exchanges between the F=1 states and the F=0 state. For a sweep tuning from above to below the resonances the state $|0,0\rangle$ is first swapped with $|1,1\rangle$, then $|1,0\rangle$ and finally $|1,-1\rangle$.

cavites, whose FSR is twice the Zeeman splitting, in a polarization interferometer (Fig. 6) resuling in a state $|H,\omega_1\rangle_{\text{photon}}\,|1,+1\rangle_{\text{ion}} + |V,\omega_2\rangle_{\text{photon}}\,|1,-1\rangle_{\text{ion}}$, similar to that used in [18]. A reduction of 100 in the polarization blurring related error rate can be obtained for a Yb^+ ion in a 67 gauss field (160 MHz Zeeman splitting) using two Fabry-Perot cavities of finesse 16 and 320 MHz FSR. Drawbacks to this resolved Zeeman splitting approach include an increase in the complexity of the cooling and readout, as well as the need to stabilize the phase imparted by the filtering interferometer. If purely polarization basis photonic qubits are desired an acousto-optic modulator could be introduced into one of the interferometer arms to equalize the optical frequency difference.

3.3 Chromatic aberration in phase Fresnel lenses

The large change in focal length with wavelength or chromatic dispersion of phase Fresnel lenses is well known to optical engineers. It cannot be practically compensated with conventional refractive optics for high NA PFLs. While this is not an issue for photonic qubits encoded in the polarization basis [8], it does present a concern for those that have been encoded with the hyperfine frequency difference [17]. For a small change in wavelength the focal shift of a PFL is $\Delta f \approx f_0 \Delta\lambda/\lambda_0$.

In $^{171}Yb^+$ the 12.6 GHz ground state hyperfine splitting corresponds to a fractional difference in wavelength of $\Delta\lambda/\lambda = 15 \times 10^{-6}$ on the 369.5 nm transition line. For the characterized f=3 mm PFL this results in a small but non-negligible focal shift of 47 nm or 5% of the Rayleigh range. The chromatic focal shift Δf is less than the nominal Rayleigh range (or depth of focus) $z_R = 4\lambda/\left(\pi \text{NA}^2\right)$ for PFLs with focal length $f < 4\lambda^2/\left(\pi\Delta\lambda\text{NA}^2\right)$. For $^{171}Yb^+$ ions with an 0.9 NA lens this criteria is satisfied for focal lengths less than 39 mm, and hence should not present a problem for integrated PFL arrays. For large departures from the design wavelength the aberration corrections in the PFL design cease to be valid and a chromatically dependent spherical aberration limits the spot size. We have observed for $\Delta\lambda$= 1 nm that this effect limited the beam quality factor to $M^2 \geq 1.7$, well above the diffraction limit.

4 Fresnel lenses for large-scale ion-trap quantum computing

Most proposals for large-scale ion-trap quantum computing (QC) envisage the use of a large array of ion traps and the collection of ion fluorescence from many sites of the trap array [9, 19, 20, 21]. Trapping and transport of ions in microfabricated trap arrays is now routine [5] and current trap fabrication technology is suited to the production of extremely large trap arrays [22]. These same sophisticated ion-trap experiments collect ion fluorescence using complex, bulky multi-element objective lenses that must be aligned manually, a technology that is hardly scalable at all. A new approach will be required for highly parallel fluorescence collection.

Arrays of phase Fresnel lenses are an excellent candidate for scalable fluorescence collection optics. We have shown how single PFLs can significantly improve collection efficiency and coherent mode conversion over present-day optics. In addition, large PFL arrays can be microfabricated on a single substrate, so that only a single alignment step is needed for high-efficiency collimation of light from a large number of trap sites. These ideas were already realised for optical communications as long ago as the 1980s, with the fabrication of high-

density optical interconnects based on PFL arrays [23]. This already mature technology, improved for higher numerical aperture and UV wavelengths, can bring massively parallel fluorescence collection to ion-trap QC.

Alternative methods of fluorescence collection from a trap array include the use of a single multi-element objective to image the entire array at once [10] or the use of an array of conventional microlenses. In the first case, the semiconductor industry has indeed demonstrated lithographic imaging with submicron resolution over large flat field of 25 mm in diameter [24], but the large, multi-element imaging lenses involved are the result of an extensive design effort, concentrated at a few wavelengths of interest to that industry, that is unlikely to be replicated in quantum computing research. Indeed, these imaging lenses might even be replaced by PFL arrays in semiconductor lithography itself [25].

High NA refractive microlens arrays appear to share desirable features with PFL arrays, but these devices are fabricated from materials which are either not vacuum compatible or strongly absorbing at the UV wavelengths relevant to ion-trap quantum computing. For materials that meet both the UV and vacuum compatibility criterial, microlens arrays have been demonstrated up to NA of 0.3 [26], with diffraction-limited performance below NA of 0.2 [27]. The photoresists and epoxies used in fabricating high NA microlenses [26] are designed to be activated by UV light and hence make them poor choices as materials for UV optics. In addition, while microlenses with NA's of up to 0.85 [28] have been demonstrated, these lenses are composed of only a few refracting surfaces and do not exhibit diffraction-limited performance. The advantages of large NA, diffraction-limited performance, vacuum compatibility, and low UV absorption make PFL arrays a superior choice for massively parallel ion trap QC.

4.1 Highly parallel, efficient detection for quantum error correction

Every qubit in a large-scale quantum computer will require frequent and repeated error correction, and thus frequent and accurate measurement, to avoid decoherence. For this reason, calculations of fault-tolerance error thresholds for large-scale QC generally assume that error correction can be applied in parallel to all logical qubits [29]. A fault-tolerant ion-trap quantum computer is expected to require photon collection efficiency p_{coll} of at least 5% with parallel detection at $\sim 10^3$ sites [11], corresponding to NA ≥ 0.44 for an ideal lens under the top-hat criterion. Here we have assumed a detection quantum efficiency of 20%, as is typical for ion-trap experiments [17].

PFL arrays are well suited to highly parallel, efficient detection. The e-beam lithography process for PFL array fabrication is extremely flexible in terms of design wavelength and focal length, since these are controlled by changing the groove spacing and depth. The only factors limiting the NA of the PFL array are 1) the distance between detection regions, which sets the maximum useful clear aperture and 2) the minimum allowable distance to the PFL array owing to proximity effects on the ion-trapping fields, which sets the minimum focal length. A trap optimally designed for ion shuttling should have segments of length $\approx d/2$, where d is the distance to the nearest electrode [30]. At least seven segments per trap site are required for a square 2D trap array, since each trap site should be able to split an ion crystal and

each junction must be able to direct ions along any desired path. An efficient quantum error-correcting code requires less than 1/5 of the physical qubits to be measured [11], so detection is required at less than 1/5 of the trap sites. We then find a separation of $> 7.8d$ between detection regions. We take a focal length for the Fresnel lens of $\sim 3d$, which has previously been found to be sufficiently far that surface charge proximity effects on the trap fields are negligible [31]. As for other proximity effects, the fused silica used for our test PFL is known to have low RF loss and should therefore not adversely impact the trapping potential. We then find that the useful NA of a PFL array is at least 0.6 (the NA of our test lens), and can be substantially higher. At NA = 0.6, the diffraction efficiency can easily exceed 60% [13], so we anticipate a collection efficiency of $p_{coll} \geq 8\%$ at each site, sufficient for fault-tolerant QC. In contrast, microlens arrays are limited to a collection efficiency of 3.4%, assuming a maximum NA= 0.3 [26] and no losses.

4.2 Coherent mode conversion for quantum communication

We now consider probabilistic quantum communication by networking together remote ions with photons [32], which exploits the entanglement between the ion state and the outgoing photon state created by spontaneous emission. Recent experiments have created remote ion-ion entanglement by the probabilistic detection of individual fluorescence photons emitted by two widely separated ions [17, 18]. An array of small ion-trap quantum registers, supplemented by remote entanglement of this kind, could support the processing needs of a distributed quantum network [33].

The phase Fresnel lens is an outstanding technology for massively parallel ion-photon networking because of its unique potential for high p_{coh}. Remote entanglement is a scarce resource in large-scale QC, so we anticipate that a networking architecture will favor high p_{coh} over high density of detection regions, especially since ions need not be shuttled between sites for logic operations. In the coincident-detection scheme described above, the leading sources of error are the imperfect polarization of the excitation laser and the imperfect filtering of photons, and the estimated error rate is less than 0.01 even at NA close to 1. Rigorous coupled-wave calculations for a four-level PFL show that the diffraction efficiency can exceed 50% at an NA of 0.8 [13], for which the collection efficiency of σ_+/σ_- photons is 25%. Absorption losses from coating such a PFL with 20 nm of the transparent conductor indium tin oxide, sufficient to reduce the sheet resistance to 1kΩ/square and prevent stray charge build up [14], would reduce the efficiency by only 12% [13]. Our measured M^2 at NA = 0.64 is less than 1.1, and the imaging resolution of PFLs at 400 nm conforms to the theoretical prediction for NA up to 0.85 [12], so we conservatively estimate $M^2 < 1.5$ at NA of 0.8. Then $p_{coh} = 6\%$, giving a 200-fold increase of remote entanglement rate over [18].

5 Conclusion

Large numerical aperture optics are crucial to scaling up ion-trap quantum computing. We have shown how phase Fresnel lens arrays are a superior alternative to conventional multi-element lenses or refractive microlens arrays for integration with chip type ion traps. In particular, coincident-detection-based remote ion-ion entanglement schemes benefit from PFLs since the entanglement rate scales as NA^4 and depends on high spatial mode quality. We have demonstrated the optical viability of a PFL as a large NA collection and coherent cou-

pling optic for ion-trap quantum computing with the measurement of a diffraction-limited sub-micron spot. The chromatic aberrations in PFLs were quantified and found not to limit performance at high NA for typical trap configurations. In addition we have proposed two fidelity enhancement techniques to the ion-photon entanglement scheme based on $\sigma^{\pm}$ polarized photons from a Raman transition.

Acknowledgments

We would like to thank the Australian Research Council (ARC) for their support of this research through Discovery Project grants DP0773354 (Kielpinski) and DP0877936 (Streed) as well as Prof. Howard Wiseman's Federation Fellowship grant FF0458313. This work was also supported by the US Air Force Office of Scientific Research under contract FA4869-06-1-0045. E. Streed acknowledges the support of an Australian Postdoctoral Fellowship from the ARC. We thank Prof. Wolfgang Lange for helpful discussions. Phase Fresnel lenses were fabricated by Margit Ferstl at the Heinrich-Hertz-Institut of the Fraunhofer-Institut für Nachrichtentechnik in Germany.

References

1. P. W. Shor (1994), *Polynomial-Time Algorithms for Prime Factorization and Discrete Logarithms on a Quantum Computer* Proc 35th Ann Symp Found Comp Sci (IEEE Computer Society, Los Alamitos, CA), p.124.
2. L. K. Grover (1997) *Quantum Mechanics Helps in Searching for a Needle in a Haystack* Phys. Rev. Lett. Vol 79, 325.
3. C.H. Bennett and G. Brassard (1984) *Quantum Cryptography: Public Key Distribution and Coin Tossing* Proc Intl Conf Comp Sys Sig Proc,(IEEE Bangalore India) pp 175-179.
4. D Kielpinski (2003) *A small trapped-ion quantum register* J. Opt. B: Quantum Semiclass. Opt. 5 pp R121-R135.
5. D. Leibfried, D. J. Wineland, R. B. Blakestad, J. J. Bollinger, J. Britton, J. Chiaverini, R. J. Epstein,W. M. Itano, J. D. Jost, E. Knill, C. Langer, R. Ozeri, R. Reichle, S. Seidelin, N. Shiga, J. H. Wesenberg (2007) *Towards scaling up trapped ion quantum information processing* Hyperfine Interact Vol 174 pp 17
6. J. Benhelm, G. Kirchmair, C. F. Roos, and R. Blatt (2008) *Towards fault-tolerant quantum computing with trapped ions* arXiv:0803.2798v1 [quant-ph].
7. K.-A. Brickman, P.C. Haljan, P. J. Lee, M. Acton, L. Deslauriers, and C. Monroe (2005) *Implementation of Grover's quantum search algorithm in a scalable system* Phys. Rev. A Vol 72 050306(R).
8. B. B. Blinov, D. L. Moehring, L.-M. Duan, and C. Monroe (2004) *Observation of entanglement between a single trapped atom and a single photon* Nature Vol 428, pp. 153-157.
9. D. Kielpinski, C.R. Monroe, and D.J. Wineland (2002) *Architecture for a large-scale ion-trap quantum computer* Nature, Vol. 417, pp. 709.
10. J. Kim, S. Pau, Z. Ma, H. R. McLellan, J.V. Gates, A. Kornblit, and R. E. Slusher (2005) *System design for large-scale ion trap quantum information processor* Quant. Inf. Comp., Vol.5, pp. 171-183.
11. A. M. Steane (2007), *How to build a 300 bit, 1 Giga-operation quantum computer* Quant. Inf. Comput., Vol.7, pp. 171-183.
12. R. Menon, D. Gil, and H. I. Smith (2006) *Experimental characterization of focusing by high-numerical-aperture zone plates* J. Opt. Soc. Am. A Vol 23, pp. 567-571.
13. A. A. Cruz-Cabrera, S. A. Kemme, J. R. Wendt, D. Kielpinski, E. W. Streed, T. R. Carter, S. Samora (2007) *High Efficiency DOEs at Large Diffraction Angles for Quantum Information and*

Computing Architectures Proc. of SPIE, 6482, 648209.
14. M. J. Alam and D. C. Cameron (2000) *Optical and electrical properties of transparent conductive ITO thin films deposited by sol-gel process* Thin Solid Films Vol. 377-278 pp. 455-459
15. J. J. Chapman, B. G. Norton, E. W. Streed, and D. Kielpinski (2008) *Measurement of focusing properties for high numerical aperture optics using an automated submicron beamprofiler* Rev. Sci. Instr. Vol. 79 095106.
16. A. E. Siegman, G. Nemes, and J. Serna (1998) *How to (Maybe) Measure Laser Beam Quality* DPSS (Diode Pumped Solid State) Lasers: Applications and Issues, M. Dowley, ed., Vol. 17 of OSA Trends in Optics and Photonics (Optical Society of America, 1998).
17. D. L. Moehring, P. Maunz, S. Olmschenk, K. C. Younge, D. N. Matsukevich, L.-M. Duan, and C. Monroe (2007) *Entanglement of single-atom quantum bits at a distance* Nature 449, 68.
18. D. N. Matsukevich, P. Maunz, D. L. Moehring, S. Olmschenk, and C. Monroe (2008) *Bell Inequality Violation with Two Remote Atomic Qubits* Phys. Rev. Lett. Vol. 100, 150404
19. D. J. Wineland, C. Monroe, W. M. Itano, D. Leibfried, B. E. King, and D. M. Meekhof (1998) *Experimental Issues in Coherent Quantum-State Manipulation of Trapped Atomic Ions* J. Res. NIST Vol. 103, pp. 259-328.
20. L.-M. Duan, B. B. Blinov, D. L. Moehring, and C. Monroe (2004) *Scalable trapped ion quantum computation with a probabilistic ion-photon mapping* Quant. Inf. Comp. Vol. 4, pp. 165-173.
21. L.-M. Duan (2004) *Scaling ion trap quantum computation through fast quantum gates* Phys. Rev. Lett. Vol. 93, 100502.
22. S. Seidelin, J. Chiaverini, R. Reichle, J. J. Bollinger, D. Leibfried, J. Britton, J. H. Wesenberg, R. B. Blakestad, R. J. Epstein, D. B. Hume, W. M. Itano, J. D. Jost, C. Langer, R. Ozeri, N. Shiga, and D. J. Wineland (2006) *Microfabricated Surface-Electrode Ion Trap for Scalable Quantum Information Processing* Phys. Rev. Lett. Vol. 96, 253003.
23. L.A. Hornak (1987) *Fresnel phase plate lenses for through-wafer optical interconnections* Appl. Opt. Vol. 26, pp. 3649-3654.
24. Carl Zeiss Starlith series Lithographic systems product literature for 365 nm optics. "The image field is 26 mm x 33 mm, and the numerical aperture (NA) can be adjusted from 0.45 to 0.65." www.zeiss.com
25. D. Gil, R. Menon, and H. I. Smith (2004) *The promise of diffractive optics in maskless lithography* Microelec. Eng. Vol. 73-74, pp. 35-41.
26. H Ottevaere , R Cox , H P Herzig , T Miyashita , K Naessens , M Taghizadeh, R Völkel, H J Woo and H Thienpont (2006) *Comparing glass and plastic refractive microlenses fabricated with different technologies* J. Opt. A Vol 8, pp S407-S429.
27. F. Merenda, J. Rohner, J.-M. Fournier and R.-P. Salathé (2007) *Miniaturized high-NA focusing-mirror multiple optical tweezers* Opt. Exp. Vol. 15, pp 6075-6086.
28. T. Miyashita (2005) *Handbook of Optical Interconnects, Ch 2, The Microlens* ed S. Kawai Taylor & Francis.
29. A.M. Steane (2003) *Overhead and noise threshold of fault-tolerant quantum error correction* Phys. Rev. A Vol. 68, 042322
30. J.P. Home and A.M. Steane (2006) *Electrode configurations for fast separation of trapped ions* Quant. Inf. Comp. Vol. 6, pp. 289-325
31. M. Keller (2004) *Quantenoptik mit gespeicherten* $^{40}Ca^{+}$*-Ionen* Ph.D thesis, Ludwig-Maximilians-Universität München, p. 113 ff.
32. D. L. Moehring, M. J. Madsen, K. C. Younge, R. N. Kohn, Jr., P. Maunz, L.-M. Duan, C. Monroe, and B. Blinov (2007) *Quantum Networking with Photons and Trapped Atoms* J. Opt. Soc. Am. B 24, 300.
33. H. J. Kimble (2008) *The quantum internet* Nature Vol 453 pp 1023-1030